Physical modeling of gelatinous zooplankton sinking in the deep global ocean

M. Ličer [1,2], M. Vodopivec [2], G. J. Herndl[3,4], T. Tinta [2]

[1]Slovenian Environment Agency, Ljubljana, Slovenia
[2]National Institute of Biology, Ljubljana, Slovenia
[3]Department of Functional and Evolutionary Ecology, Bio-Oceanography and Marine Biology Unit, University of Vienna, Vienna, Austria
[4]NIOZ, Department of Marine Microbiology and Biogeochemistry, Royal Netherlands Institute for Sea Research, Den Burg, The Netherlands

Key Points:

- We formulate a dynamically consistent physical model of GZ sinking
- We solve model equations for entire global ocean
- Substantial carbon export to deep ocean is only possible in the polar ocean

Corresponding author: Matjaž Ličer, `matjaz.licer@nib.si`

Abstract

Decaying gelatinous zooplankton (GZ) originating from surface waters has been proposed as a possible major contributor to the biological carbon pump. However, studies arrived at largely diverging conclusions concerning the role of decaying GZ as organic matter supply for the deep-sea heterotrophic biota. We complement previous approaches to GZ sinking by proposing the first dynamically consistent physical model coupling GZ sinking speed and its mass. We evaluate GZ contribution to deep-ocean carbon sequestration and to the soft-tissue carbon pump by solving the model equations on the global ocean grid employing monthly climatological temperature fields and published exponential and linear temperature dependencies of mass decay rates. We present the global ocean distribution of the fraction of GZ-mass sinking out of the euphotic zone (200 m depth), twilight zone (1000 m depth) and the fraction of mass reaching the global ocean floor. Solutions in the upper water column are strongly dependent on the mass decay rate. Since most of the decay happens in the initial phase of the sinking process, the sinking-decay coupling exerts a substantial impact on sinking rates but has limited effect on the fraction of mass reaching the bathypelagic and abyssal ocean. Our model approach indicates that there are substantial latitudinal differences in the potential supply of GZ detrital matter to the deep sea. While at low latitudes only negligible amounts of GZ biomass are deposited at the ocean floor, high latitudes allow for substantial GZ detrital mass transport to depths below 1000 m.

Plain Language Summary

Decaying zooplankton sinking into deep ocean has been proposed as a possible major contributor to the vertical carbon flux to ocean floor. We formulate the first physical model which includes impact of organism decay on its sinking speed. We use this model to create global estimates of how much zooplankton can reach deep ocean and the ocean floor. We show that in equatorial and mid-latitude ocean most of organisms completely decay before reaching depths over 1000 m and the ocean floor. In the polar ocean, however, a lot of zooplankton mass can reach the ocean floor due to lower ocean temperatures.

1 Introduction

Atmospheric carbon enters the ocean via photosynthesis and, following a chain of diverse biochemical reactions, ends up in a plethora of carbon-containing compounds stored in the biomass of different organisms. A fraction (10-30 %) of this organic carbon is exported into the ocean's interior either via sinking, downwelling of surface waters (rich in dissolved organic matter) or active vertical migration of organism (Herndl & Reinthaler, 2013; P. W. Boyd et al., 2019; Iversen, 2023). Collectively, these mechanisms are known as the biological carbon pump (Herndl & Reinthaler, 2013; P. W. Boyd et al., 2019). The biological processing of the particulate organic matter during its sinking through the water column affects the global carbon cycle and ultimately, the global climate. However, there is a known mismatch between surface-ocean carbon supply exported to the ocean's interior via sinking particulate organic carbon (POC) and dissolved organic carbon (DOC) advection, and the carbon demand by mesopelagic and bathypelagic zooplankton and heterotrophic microbes (Burd et al., 2010). It has been recently suggested that gelatinous zooplankton (GZ), which has been largely overlooked as a source of carbon for the deep-sea biota, could represent one of the missing pieces in this puzzle (Steinberg & Landry, 2017).

GZ, specifically the cnidarian subphylum *Medusozoa*, the phylum *Ctenophora* and pelagic tunicates (*Thaliacea*, phylum *Chordata*), inhabit a wide range of marine ecosystems and are responsible for a substantial amount of pelagic secondary production (i.e., net GZ production estimated at 3.9–5.8 Pg C y^{-1} in the epipelagic ocean (Luo et al.,

2020)), occasionally forming large blooms with high biomass. Once GZ die off, their carcasses can face different fates: they can be (i) consumed or fragmented by predators and scavengers, (ii) degraded by pelagic communities (macro and micro-organism), (iii) sink intact through the water column as 'jelly-falls' and/or (iv) be degraded by benthic communities once reaching the seafloor (Tinta et al., 2021). There are many factors determining the fate of GZ-carbon in the ocean, with many unknowns that need to be addressed to accurately incorporate GZ into the ocean carbon budgets, as recently suggested (Tinta et al., 2021).

The global jellyfish biomass estimates range from 0.1 PgC to 3.1 PgC (Lucas et al., 2014; Bar-On et al., 2018; Luo et al., 2020; Wright et al., 2021). Using a value of 0.51 PgC as the total GZ biomass, it has been recently estimated that total gelatinous zooplankton POC export at 100 m is equivalent to 32–40% of the total global POC export (Luo et al., 2020). Furthermore, it has been estimated that sinking GZ export resulted in a high transfer efficiency of 38–62% to 1000 m depth, and 25–40% to the seafloor(Lebrato et al., 2019). This indicates that sinking GZ carcasses could be some of the most important contributors to carbon sequestration in the deep ocean (i.e., being an important component of the soft-tissue carbon pump).

However, these estimates are based on studies, which mostly considered a scenario in which GZ carcasses rapidly sink through the water column, while being subjected to degradation by different pelagic organisms (Lebrato et al., 2013, 2019). The sinking speed is crucial in determining the amount of GZ-carbon reaching different depths of the ocean and the values used in previous studies, i.e., 800-1200 m d^{-1} for *Chordata*, 900-1100 m d^{-1} for *Cnidaria* and 500-1300 m d^{-1} for *Ctenophora* (Lebrato et al., 2013, 2019), were obtained in relatively simple laboratory experiments, with shortcomings previously discussed (Tinta et al., 2021). However, these are the only estimates on the sinking speeds of GZ carcasses to date, and were hence used as initial values for the sinking speed in this study as well.

In this paper we complement numerical approaches from previous studies (Lebrato et al., 2013, 2019). First, we address the fact that the decay of organisms affects sinking speed due to changing mass, which modifies the ratio between forces of gravity, buoyancy and drag. We solved these equations on a global ocean grid using exponential and linear GZ mass decay rates (Lebrato et al., 2019) over several exit depths and several initial sinking speeds. We present two-dimensional maps of solutions and their zonal means, along with local solutions at several relevant global ocean locations which correspond to high GZ biomass.

2 Physical model of sinking and decaying GZ

This sections describes the model equations. Following a previous publication (Lebrato et al., 2019) we describe the decay rate as

$$\frac{\mathrm{d}m}{\mathrm{d}t} = -k(T)m, \tag{1}$$

where the coefficient $k(T)$ (hereafter referred to as decay rate) was determined from observations following either a linear or an exponential function of the in-situ temperature $T(z)$. In the linear case, k is

$$k_{lin} = 0.064\,^{\circ}C^{-1}\,\mathrm{d}^{-1}T(z) + 0.02\,\mathrm{d}^{-1}, \tag{2}$$

while in the exponential case, k is estimated as

$$k_{exp} = 0.140\,\mathrm{d}^{-1}\exp[0.145\,^{\circ}C^{-1}\cdot T(z)]. \tag{3}$$

As noted earlier (Lebrato et al., 2019), k_{exp} leads to a rapid decay at the surface. To remedy this, k_{lin} is proposed as a more moderate decay function.

Equation (1) and the two decay rates (k_{exp} and k_{lin}) already allow estimating organism decay in its initial phase. Shortly after organism death the solution to Equation (1) is

$$m = m_0 e^{-k_0 t} = m_0 e^{-t/\tau}; \tau = k_0^{-1}, \tag{4}$$

where m_0 and k_0 are initial mass and initial value of k, respectively. Hence inverse decay rate $\tau = k_0^{-1}$ plays the role of the typical timescale during which the decaying mass drops by a factor of e to $\sim 0.36\, m_0$. In case of an exit depth near the surface and at typical equatorial sea surface temperature of $25°C$, decay rates (2) and (3) lead to $k_{lin,0}^{-1} \sim$ 15 h and $k_{exp,0}^{-1} \sim 5$ h. Within 24 h, traveling at $w \sim 1000$ m d^{-1}, the organism will have sunk by about a 1000 m. We can therefore estimate that in the first 1000 m, its mass will decay to about $\exp(-24/5)\, m_0 \sim 0.01\, m_0$ in case of exponential decay rate and, similarly, to about $\exp(-24/15)\, m_0 \sim 0.20\, m_0$ in case of linear decay rate. These simple estimates will serve as a quick benchmark for the validity of full solutions, presented below.

Assuming the spherical shape of the GZ, Newton's law for vertical motion takes the form (with vertical axis oriented upwards):

$$\rho_{gz} V \frac{\mathrm{dw}}{\mathrm{d}t} = -\rho_{gz} V g + \rho_{oc} V g + \frac{1}{2} \rho_{oc} C_D \pi r^2 \mathrm{w}^2 \tag{5}$$

where w is the total vertical speed of the sinking organism, and the terms on the right-hand side of the equation are gravity, buoyancy and friction (adopted from (Yang et al., 2018) with zero vertical background flow). $\rho_{oc} = 1025$ kg m^{-3} and ρ_{gz} are ocean and GZ mass densities. As we will show below, we do not need to know the actual value of ρ_{gz} as long as we know the sinking speeds which were reported elsewhere (Lebrato et al., 2019). $V(t) = m(t)/\rho_{gz}$ and $r(t) = (3m(t)/4\pi\rho_{gz})^{1/3}$ are the volume and the radius of the GZ, respectively. Both values change as GZ mass $m(t)$ diminishes due to microbial decay, g is gravitational acceleration, C_D is the drag coefficient of the GZ shape. We demonstrate below that the sinking dynamics is not governed by C_D or ρ_{gz} individually, but rather by a product of powers of C_D and ρ_{gz} - and this product is calculated directly from observations reported in previous publication (Lebrato et al., 2019) without making any specific assumption about the value of either C_D or ρ_{gz}.

Assuming that the time needed for sinking organism to reach its terminal sinking speed, which we denote with the symbol w, is much shorter than the timescale of the organism's decay, we can set $\mathrm{dw}/\mathrm{d}t = 0$ in Equation (5). In other words, we assume that the decaying organism is always traveling at its equilibrium terminal speed w while we are still allowing this terminal speed $w(t)$ to change slowly (on decay timescales) as the organism's mass $m(t)$ decreases.

Condition $\mathrm{dw}/\mathrm{d}t = 0$ in Equation (5) leads to relation

$$\frac{1}{2} \rho_{oc} C_D \pi r^2(t) w^2(t) = (\rho_{gz} - \rho_{oc}) g (4\pi/3) r^3(t), \tag{6}$$

which, since $r = (3m/4\pi\rho_{gz})^{1/3}$, yields the following expression for terminal speed

$$w(t) = \kappa m^{1/6}, \tag{7}$$

where

$$\kappa = \left[\frac{8g}{3C_D} \left(\frac{\rho_{gz} - \rho_{oc}}{\rho_{oc}} \right) \right]^{\frac{1}{2}} \left(\frac{3}{4\pi\rho_{gz}} \right)^{\frac{1}{6}} \tag{8}$$

is a constant numerical parameter. This parameter can be determined directly from observed vertical sinking speeds reported in (Lebrato et al., 2019) without knowing anything specific about C_D or ρ_{gz}. Observations of sinking speeds in (Lebrato et al., 2019) can be taken as a reliable estimates of the order of magnitude of the initial sinking speed at time $t = 0$, which we denote as w_0. Initial GZ mass at time $t = 0$ will be denoted as $m(0) = m_0$. Together with equation (7) these initial conditions yield

$$\kappa = w_0 m_0^{-1/6}. \tag{9}$$

Equation (7) thus simplifies to

$$w(t) = w_0 \left[\frac{m(z(t))}{m_0}\right]^{1/6}, \tag{10}$$

which clearly satisfies the initial condition $w(t)|_{t=0} = w_0$ and shows that w/w_0 at depth z equals the sixth root of the fraction of mass at depth z. Since $w(t) = \mathrm{d}z/\mathrm{d}t$, the system we need to solve is an initial value problem in the form of two coupled non-linear ODEs:

$$\frac{\mathrm{d}z}{\mathrm{d}t} = w_0 \left[\frac{m(z)}{m_0}\right]^{1/6} \tag{11}$$

$$\frac{\mathrm{d}m}{\mathrm{d}t} = -k(T(z))\, m(z) \tag{12}$$

where k is a known (see equations (2) and (3)) decay rate from (Lebrato et al., 2019) and $T(z)$ is the vertical ocean temperature profile at the sinking location. Physical content of these two equations is clear: as the GZ mass decreases according to Equation (12), its sinking rate decreases according to Equation (11). This causes a non-linear feedback loop: mass reduction causes vertical speed reduction, hence the organism spends more time in a given depth interval, causing its mass to reduce further within this depth interval. The system of equations (11)-(12) is an extension of the approach from (Lebrato et al., 2019) since it takes into account that sinking speed is not constant but varies with diminishing mass.

The system of equations (11)-(12) was numerically integrated using Python's `odeint` solver from `scipy` library, which is a wrapper to the explicit LSODA solver (Petzold, 1983) implemented in the FORTRAN library ODEPACK (Hindmarsh, 1983). The system was solved over a global regular latitude-longitude grid with a 1-degree horizontal resolution. At each grid point, the exit depth was set i) to the mid-euphotic zone at -100 m, and ii) to the bottom of the twilight zone at -1000 m. Initial sinking speeds were set to 500, 1000 and 1500 m d^{-1}. Initial mass was set to $m_0 = 1.0$ kg. Starting with the same initial mass in each grid point allows us to separately gauge the temperature, decay rate and initial sinking speed impact on sinking dynamics and allows for comparisons of idealized carbon export efficiency between different regions of the global ocean. Ocean temperature profiles $T(z)$ were obtained from Copernicus CMEMS Climatology GLOBAL_REANALYSIS_001_030 product and remapped to our model grid using nearest neighbor interpolation at each grid point. Subzero water temperatures in the polar regions were set to zero degrees Celsius during decay rate computation (2) and (3), yielding constant values of $k_{lin} \sim 0.02$ d^{-1} and $k_{exp} \sim 0.14$ d^{-1}. Global bathymetry used to compute the fractions of mass at ocean floor was the NOAA ETOPO2 Dataset (Center, 2006) [access date: September 13, 2023].

3 Results and discussion

3.1 Local solutions at several locations with high GZ biomass

The vertical profiles to the winter solutions to the system (11)-(12) for the exit depth of 100 m and an initial sinking speed of 1000 m d^{-1} are shown here only for selected locations corresponding to regions with high biomass concentrations as depicted in (Lebrato

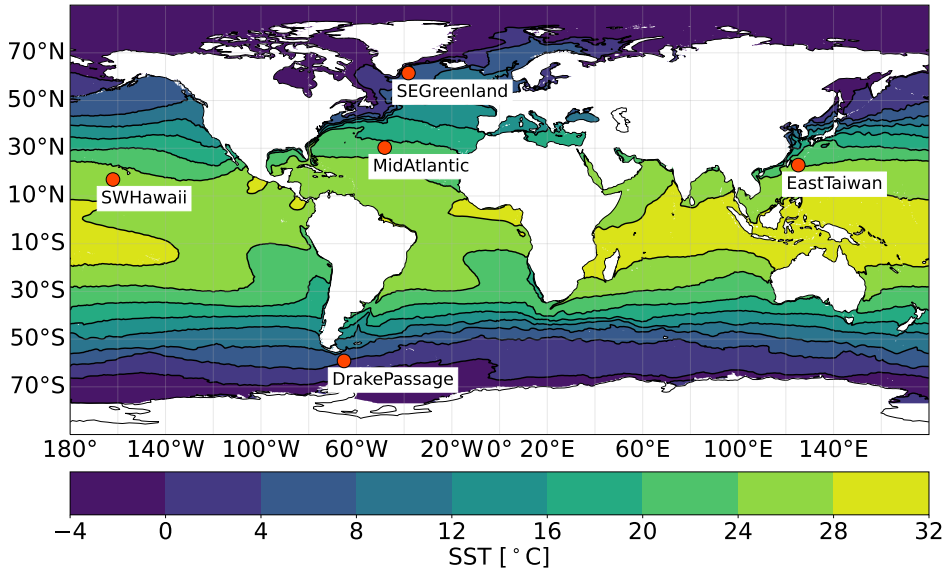

Figure 1. GZ sinking locations (red circles) which are indicative to regions of high biomass and their descriptive denotations in the paper. Background map depicts climatological mean sea surface temperature in January from Copernicus CMEMS Climatology GLOBAL_REANALYSIS_001_030 product.

et al., 2019). These locations (and their tentative names) are depicted in Figure 1, while their coordinates (latitude, longitude) are as follows: South-West of Hawaii (6.8956 N, 162.0416 W), Mid - Atlantic (30.2837 N, 48.1421 W), South-East of Greenland (61.5174 N, 38.1832 W), Drake Passage (59.1457 S, 65.1825 W), East Taiwan (22.9443 N, 125.2140 E).

Solutions for the depth dependence of mass (first column in Figure 2) in the equatorial and mid-latitude ocean (locations South West of Hawaii, Mid-Atlantic and location East of Taiwan) all exhibit a similar pattern and are remarkably consistent with decay estimates based on decay timescales k_0^{-1} from the beginning of Section 2: less than $0.01\, m_0$ reaches 1000 m depth assuming an exponential decay rate and about $0.25\, m_0$ when a linear decay rate is assumed.

In tropical and temperate regions of the ocean most of the organisms were completely degraded at 3000 m depth regardless of the decay rate. At sub-polar locations, however, a higher amount of initial mass reaches the ocean floor. At South-East of Greenland, roughly 30 % of the initial mass reaches the ocean floor, while in the Drake Passage 50-75 % of the initial mass of GZ reaches the ocean floor in the austral winter, in this case depending strongly on adopted decay rates, which lead to substantially differing decay time scales in the surface layers in the Drake passage, as depicted in the bottom row of the third column of Figure 2.

Dashed and dotted lines in the first and second columns of Figure 2 depict solutions with a fixed vertical speed of $w_0 = 1000$ m d^{-1}, i.e. solutions where sinking rate and mass decay are fully decoupled, an approach applied by previous studies (Lebrato et al., 2019). Our results show that the coupling between sinking rate and mass has a substantial impact on the sinking time to a specific depth (Figure 2, second column) but has very little effect on the fraction of mass reaching a specific depth (Figure 2, first column). In polar regions (Figure 2, bottom two rows) this is explained by the fact that decay is slow enough to not have much impact on sinking rate. In tropical and temper-

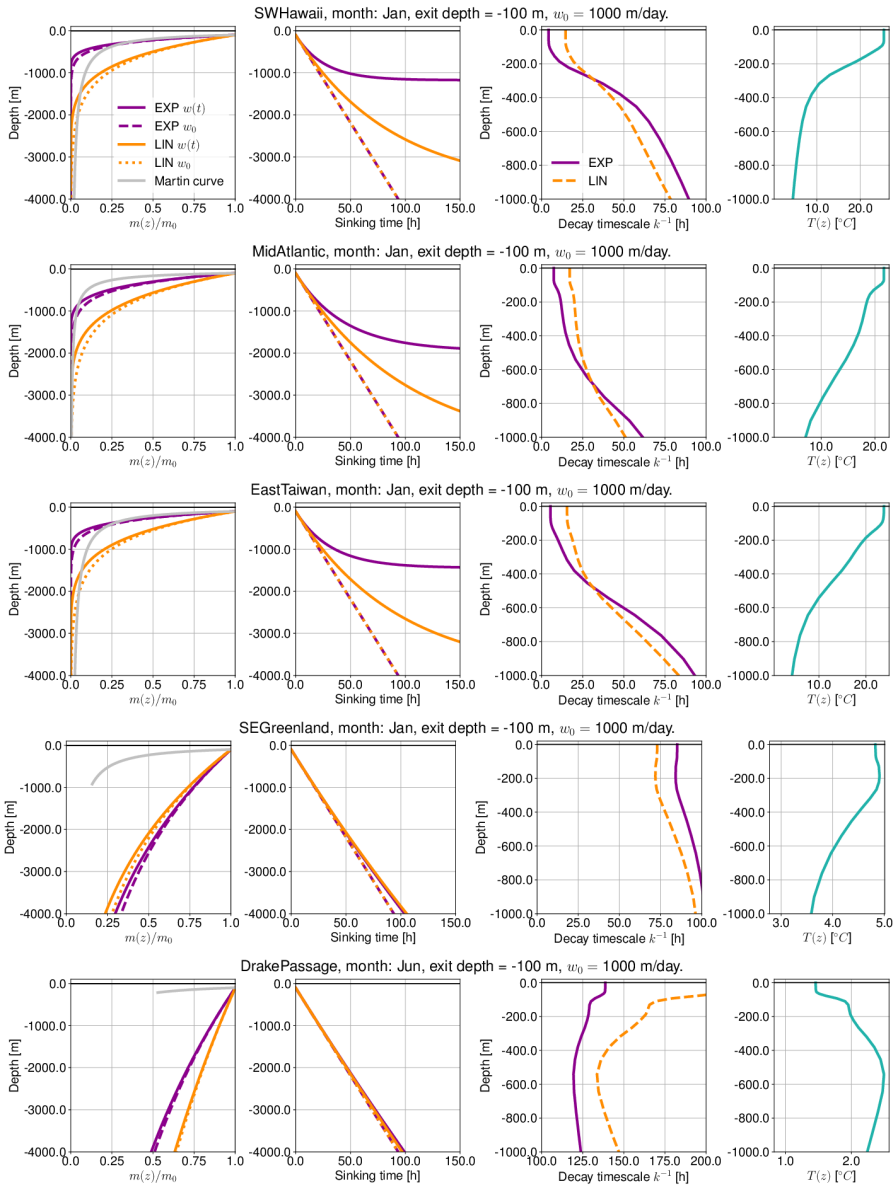

Figure 2. Solutions of the equations (11)-(12) at various locations (**rows**) in the winter (hence for Drake passage, June results are depicted). Results are shown for exit depth of 100 m and an initial sinking speed of 1000 m d^{-1}. **First column**: depth dependence of fraction of initial mass for linear and exponential decay rates. Full lines denote full solutions to system (11)-(12). Dashed lines assume a constant sinking speed of 1000 m d^{-1}. The grey line denotes the Martin curve, using location-dependent remineralization rates b from Figure 3 in (Guidi et al., 2015). Martin curve fluxes are computed for the time span of GZ sinking and are consequently truncated the moment sinking GZ organism hits the ocean floor. **Second column**: organism depth dependence on time. Full lines denote full solutions to system (11)-(12). Dashed lines assume constant sinking speed of 1000 m d^{-1}. **Third column**: depth dependence of decay timescale k^{-1} for exponential (full lines) and linear (dashed lines) decay rates. **Fourth column**: vertical temperature profile at sinking location.

ate regions (Figure 2, top three rows) however, this stems from the fact that, when starting from the same initial vertical speed of 1000 m d^{-1}, it takes about 1000-1500 vertical meters for solutions to substantially diverge (Figure 2, second column). By this depth, however, there is typically less than 20 % of the initial mass left, again preventing a major impact of mass decay on the sinking rates. Our solutions further show that an exponential decay rate effectively controls GZ carbon export in tropical and temperate regions in the top 1000 m (purple lines in top three rows of second column of Figure 2).

Grey lines in the first column of Figure 2 are the widely used Martin curve (Martin et al., 1987; Guidi et al., 2015; Iversen, 2023), which describes the power-law depth-dependence of vertical remineralization fluxes $\phi(z) = \phi_0(z/z_0)^{-b}$, where $\phi(z) = m(z)w(z)$ is the vertical mass flux at depth z and $\phi_0 = m_0 w_0$ is the mass flux at some reference depth, in our case the exit depth $z_0 = 100$ m. Exponent b was shown to vary depending on many physical, chemical and biological factors and exhibits substantial spatial variability (Henson et al., 2012; Guidi et al., 2015; Middelburg, 2019; Iversen, 2023). Exponents used to compute Martin curves in Figure 2 were taken from (Guidi et al., 2015). While there is an interesting partial match with the Martin curve for the locations SW Hawaii ($b = 0.95$), Mid Atlantic ($b = 0.70$) and East Taiwan ($b = 1.0$), there are also clear discrepancies for SE Greenland ($b = 1.2$) and the Drake Passage ($b = 1.2$).

Discrepancies between the GZ mass transport and the Martin curves are not entirely unexpected. The Martin curve describes the particle flux of heterogenous organic matter such as marine snow, while the results presented in this paper represent the mass transport of a single bulk 1 kg GZ organism subjected to different decay processes. Furthermore, the equations (11) and (12) are theoretical derivations based on laboratory decay rates and sinking velocities, while the Martin curve is a best fit to *in situ* particle flux obtained from sediment traps (Middelburg, 2019), which, however, due to their design do not capture most of GZ carcasses (Luo et al., 2020). Important to consider, yet frequently not taken into account, is that the transformation of organic matter in the water column is a mixture of many biological processes, and the attenuation in the first few hundred meters of the water column is controlled by zooplankton and microorganisms, while microbes dominate the attenuation in the deeper waters (Iversen, 2023).

3.2 Gridded solutions for the global ocean

Gridded solution maps over the entire global ocean have been obtained for climatological temperature fields and for a depth of 100 m and an initial sinking speed of 1000 m d^{-1}. Results for the exit depth of 1000 m and initial sinking speeds of 500 and 1500 m d^{-1} are available in the Supplementary Material. Figure 3 depicts the fraction of mass that arrives at the bottom of the euphotic zone at 200 m. Solutions exhibit a strong meridional gradient of local vertical carbon export out of the euphotic zone. Solutions obtained using an exponential decay rate (3) indicate that at the equator 30 - 40 % of the initial mass reaches the bottom of the euphotic zone. This percentage increases to 70 % at 30° latitudes and to more than 90 % at polar latitudes beyond 60°. A similar behavior is observed for linear decay rates (2), but carbon export numbers are substantially larger: more than 80 % of the initial mass reaches the bottom of the euphotic zone in the equatorial regions, increasing to 90 % in temperate and polar regions. Thus, decay rates are higher in tropical and subtropical than in polar regions and carbon export out of euphotic zone is more efficient in polar regions.

The fraction of mass reaching the bottom of the twilight zone (1000 m) is depicted in Figure 4. If an exponential decay rate is assumed, essentially no GZ biomass reaches this depth at latitudes between 30° S and 30° N. If a linear decay is assumed, 15-30% of mass still persists at 1000 m depth at this latitudinal band. These solutions are consistent with decay timescale k_0^{-1} estimates from Section 2. Beyond this latitudinal band a strong meridional gradient exists again, where roughly 45% of the initial mass reaches

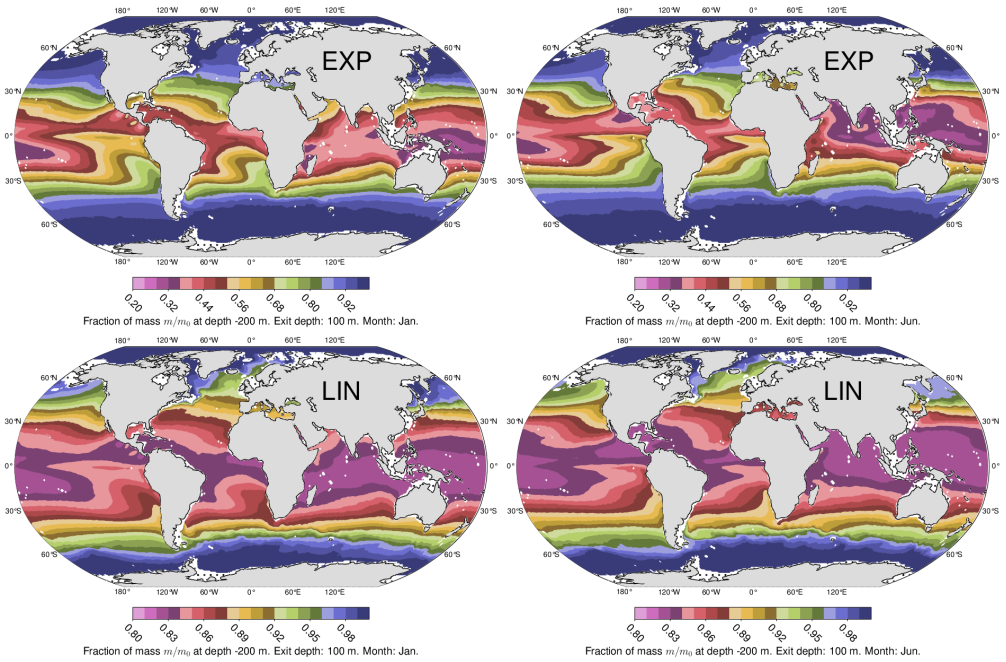

Figure 3. Fraction of mass arriving at the bottom of the euphotic zone at 200 m (from the exit depth of 100 m), starting with initial sinking speed of 1000 m d^{-1}. **Top row**: solutions with an exponential decay rate $k_{exp}(T)$. **Bottom row**: solutions with a linear decay rate $k_{lin}(T)$. **Left column**: solutions for ocean temperatures in January. **Right column**: solutions for ocean temperatures in June. Note the different color scales for exponential (top row) and linear (bottom row) decay rates.

1000 m at 45° and more than 70% of the initial mass reaches 1000 m at 70°. Low temperatures and decay timescales in the order of 100 h again allow for more than 90 % to be exported out of the twilight zone in the polar ocean.

The fraction of mass that arrives to the ocean floor at the sinking location is depicted in Figure 5. This solution indicates that regardless of the decay rate chosen, a negligible amount of mass reaches ocean floor at latitudes between 30° S and 30° N. Ocean temperatures suitable for allowing any notable amount of mass reaching the ocean floor start poleward of 45° latitude. Exponential decay rates lead to 30-45 % of initial mass at 60° parallels, while linear decay rates allow up to 75 % at similar latitudes and more than 90 % in the Southern and Arctic Ocean.

Simulations presented above were also repeated for initial sinking speeds of 500 m d^{-1} and 1500 m d^{-1} (see Supplementary material). The above conclusions remain qualitatively the same as for an initial sinking speed of 1000 m d^{-1}.

Finally, with an exit depth in the mid-euphotic zone, a negligible amount of initial mass reaches the tropical ocean floor in all sinking speed scenarios. Only the low temperatures in the polar regions allow a relevant amount of initial mass to reach the sea floor. This is clearly reflected in Figure 6, which depicts zonally averaged fields from Figures 3-5 (including initial sinking speeds 500 m d^{-1} and 1500 m d^{-1}), i.e. the zonally averaged fraction of mass reaching a specific depth (200 m, 1000m, ocean floor) at the given latitude. Results are shown only for global ocean temperatures in January, but results for June (not shown) are similar.

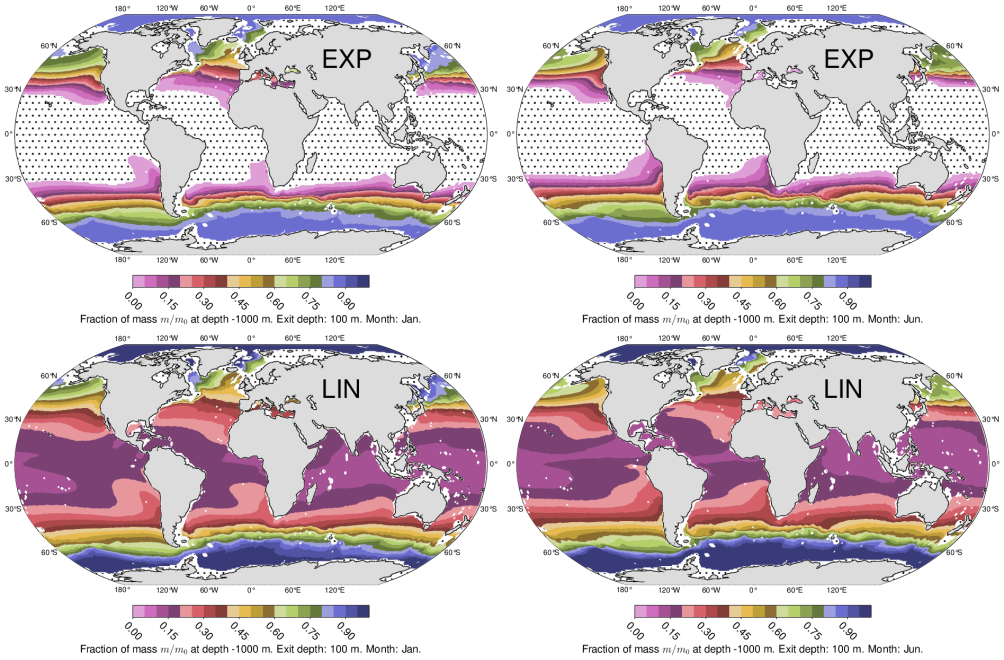

Figure 4. Same as Figure 3 but for a fraction of mass that arrives at the bottom of the twilight zone at 1000 m (from the exit depth of 100 m). Dotted regions indicate areas where less than 10^{-4} of the initial mass reached the depth of 1000 m.

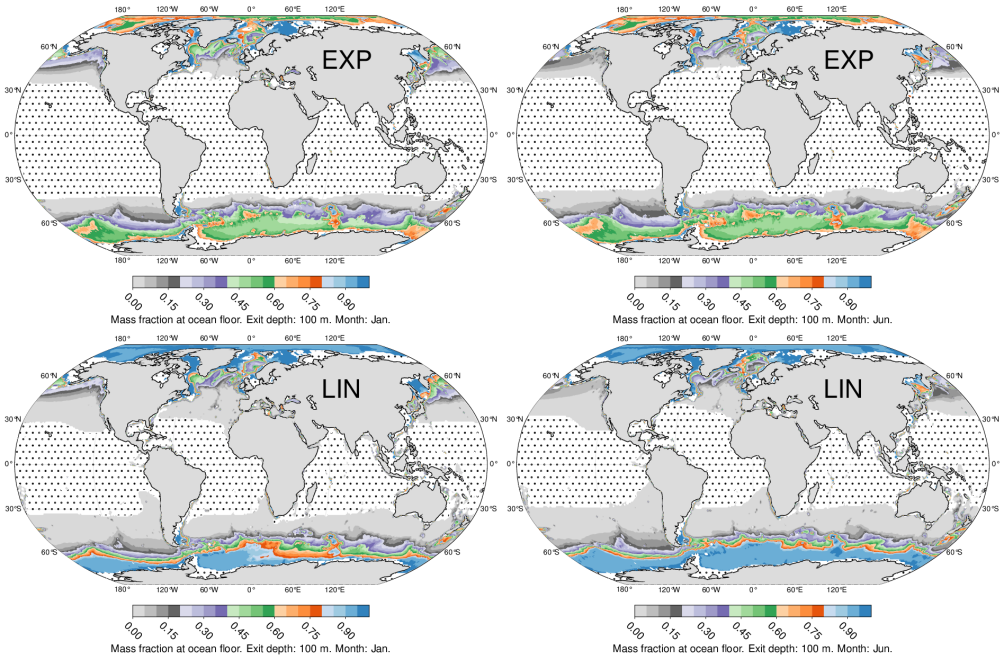

Figure 5. Same as Figure 3 but for the fraction of mass that arrives at the bottom of the ocean (from the exit depth of 100 m). Dotted regions indicate areas where less than 10^{-4} of the initial mass reached ocean floor.

The only scenario with very low, but non-zero fraction of initial mass reaching the ocean floor in tropical or temperate ocean was the scenario with an exit depth of 1000

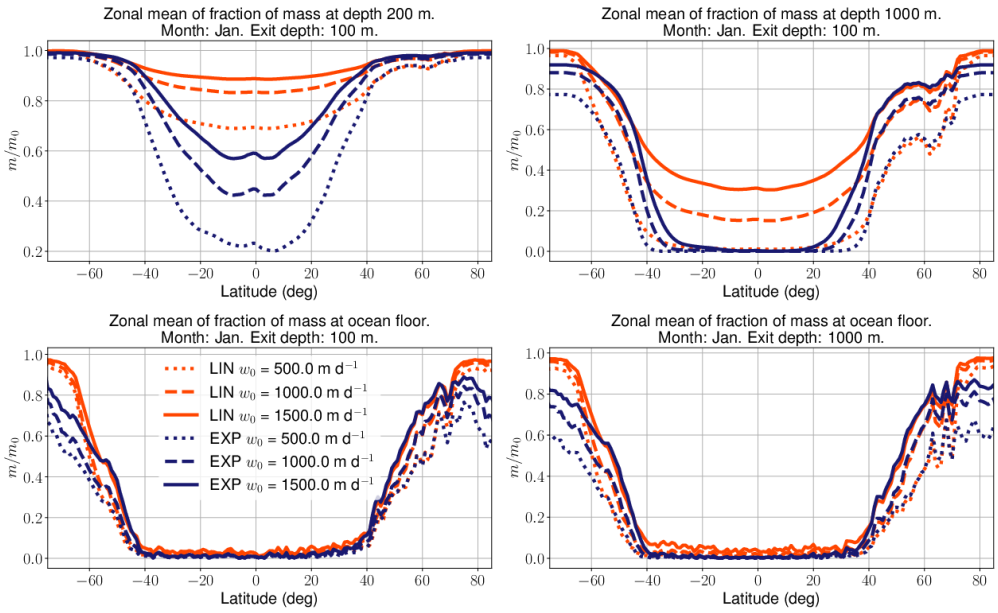

Figure 6. Zonal averages of the fraction of mass m/m_0 that reaches i) the bottom of euphotic zone at 200 m (**top left**), ii) the bottom of twilight zone at 1000 m (**top right**), and iii) the ocean floor in January from the exit depth of 100 m (**bottom left**) or from exit depth of 1000 m (**bottom right**). Orange lines correspond to linear decay, while dark blue lines depict solutions with exponential decay. Line styles differ with regard to initial sinking speed. The legend in the bottom left plot applies to all panels.

m and an initial sinking speed of 1500 m d^{-1} (Figure 6, bottom right panel). This result indicates 0 - 5 % of the initial mass reaches the bottom in the tropical and most of the temperate ocean.

These results have to be taken with caution, however, as there are substantial uncertainties in the GZ decay rates. The rates (2) and (3) are probably the best available, but have been obtained in a narrow temperature range, on a limited number of species, in specific geographic regions and at limited ocean depths, see (Tinta et al., 2021). Since our results point to a strong dependence of the GZ decay rate on ocean temperature, better constraining of these rates would help improving carbon export estimates. Furthermore, the amount of GZ biomass exported to a certain ocean depth depends also on other factors, such as the initial biomass of GZ and its specific density. Biomass of different species vary in biochemical complexity and molecular composition, which determines its bioavailability (P. Boyd & Trull, 2007; Turner, 2015; Johnson et al., 2020) and consequently their degradation and re-mineralization rates. Also, the depth where GZ die, the predation and fragmentation, the sinking velocity, seawater temperature and water column structure, the composition and functional capacity of the marine food web - all these determine the fate of GZ detrital matter ((Iversen, 2023) and references therein). Linear and exponential decay rates span over a wide range and they both indicate negligible GZ carbon export to the ocean floor in equatorial and mid-latitude ocean. The same holds for initial sinking speeds between 500 m d^{-1} and 1500 m d^{-1}. We are therefore confident that modeled carbon exports reflect actual values as long as decay rates k_{lin} and k_{exp} appropriately describe the actual decay process in the ocean.

This is however not always a valid assumption. Our results are, for example, in stark contrast with observed depositions of GZ carcasses on the ocean floor (Billett et al., 2006;

Lebrato & Jones, 2009; Lebrato et al., 2012; Hoving et al., 2023). It seems likely that the decay rates from (Lebrato et al., 2019) have a limited domain of validity due to several mechanisms, which are impossible to capture in laboratory experiments:

- The decay rates likely decrease with depth additionally to the contribution due to declining temperatures. The composition and functional capacity of microbial communities that populate GZ particles in the upper water column are likely changing with increasing depth and their metabolic activities are influenced by hydrostatic pressure and other environmental factors (Iversen, 2023; Amano et al., 2022). At the same time, the reactivity of the material is reduced with time due to remineralization and associated changes in OM composition (Henson et al., 2012; Middelburg, 2019).
- In cases of mass mortality events, the degradation capacities of surrounding ecosystem might be saturated (Tinta et al., 2021) and the decay rate should be substantially lower than observed for individual organisms. In such cases, heterotrophic microbes might be specifically important in processing this GZ detrital matter and accelerate decay.
- Observations show increasing particle settling velocities with depth (Berelson, 2002; Middelburg, 2019). There are several possible explanations for this and there is a possibility that the sinking speed of GZ detritus is increased by changes in composition, by pressure effects or by trapping other particles with higher specific density than GZ detrital matter.
- The exit depth in observed 'jelly falls' might be deeper than used in our study, which would result in larger fraction of GZ biomass transport to the ocean floor.

All the above-mentioned possibilities would result in increased vertical transport of GZ biomass. Our model, however, does not account for the fragmentation of GZ particles by zooplankton and larger organisms, which should result in a higher attenuation of GZ biomass in the epipelagic and upper mesopelagic (Iversen, 2023) and reduced GZ biomass transport. 'Jelly falls' might be a product of any or all the above explanations. They might, however, also be localized events with minor impact on the global GZ carbon export.

Our approach differs from similar studies of GZ carbon flux (Luo et al., 2020; Lebrato et al., 2019, 2013) in several respects and therefore comparison is not straightforward. Previous studies aimed at estimating actual carbon exports using available observations of global biomass distribution. Consequently, carbon exports reported in those studies are averaged quantities, weighted by the spatial distribution of GZ biomass. In other words, different spatial distribution patterns might lead to different averaged values of carbon export even if all other parameters (temperatures, decay rates, sinking speeds) are kept constant. In contrast, our GZ biomass distribution was kept constant (with an initial organism mass of 1 kg) which allowed us creating global carbon export maps where different regions of the global ocean are comparable in terms of their idealized carbon export efficiency and its dependence on ocean temperature, decay rate and initial sinking speed.

4 Conclusion

We have proposed a physical model of GZ sinking which couples GZ mass decay and its sinking speed and we have solved these equations on the global latitude-longitude grid, using a constant initial mass $m_0 = 1$ kg at each grid point to quantify how *in-situ* ocean temperatures, decay rates (Lebrato et al., 2019) and initial sinking speed impact GZ-related carbon export i) out of the euphotic zone (200 m depth), ii) out of the twilight zone (1000 m depth) and iii) carbon export to the ocean floor. In this sense, this work is an extension of previous studies which all adopt constant sinking speeds throughout the sinking process. We have shown however that while being physically consistent

and mathematically stricter, the mass-sinking speed coupling, when compared to the constant sinking speed simulations, leads to limited differences of carbon export in the order of 5% or less.

Our results indicate that the choice of a linear or exponential decay rate plays a crucial role in the upper water column and strongly impacts carbon exports out of the euphotic and twilight zones. In either case, however, a negligible amount of initial GZ mass reaches the ocean floor within the latitudinal band between 40° S and 40° N. Our results suggest that regardless of the decay rate and initial sinking speed, substantial carbon export to the ocean floor can only occur in the regions poleward of 50° latitude. This holds even in case of an exit depth of 1000 m and a fast sinking (1500 m d^{-1}) scenario.

We acknowledge that in situations, when the quantity of decaying GZ biomass exceeds the capacity of the marine food web to degrade and remineralize it, GZ carcasses can sink intact through the water column as 'jelly-falls' resulting in mass depositions at the seafloor. Nevertheless, there are very few records of mass depositions of GZ carcasses at the seafloor, and mainly in coastal systems, while only little is known for the open ocean (Billett et al., 2006; Lebrato et al., 2012; Hoving et al., 2023).

Further work is needed to better delineate GZ-carbon exports. It would certainly be beneficial to better constrain decay rates through further measurements. Gridded computations of actual carbon export estimates are ongoing by coupling the model to actual spatial distribution patterns of global ocean GZ biomass. Furthermore, mechanically and biologically induced fragmentation of GZ into several size fractions might lead to different sinking speeds. These largely overlooked procesess, albeit likely occurring in the upper water column due to physical mixing or by zooplankton (Briggs et al., 2020), would allow better constraining the GZ carbon export. Furthermore, the carbon content in our model does not change with decay, while we know that C:N ratios change due to selective microbial uptake (i.e., taking up N-compounds preferentially, resulting in C-enriched particles, e.g., [20, 21]. Present and future studies will be steps towards an improved understanding of GZ carbon and nitrogen flux estimates to different ocean depths and will allow us better constraining the amount of GZ biomass deposited at the seafloor and hence also its impact on the benthos.

5 Open Research

The coding was done in Python 3.9. The solver code, the remapped bathymetry and remapped ocean temperature datasets, needed to reproduce the results of this paper, are available under Creative Commons Attribution 4.0 International License at `https://doi.org/10.5281/zenodo.8337381`

Acknowledgments

ML and TT were supported by the financial support from the Slovenian Research Agency (research core funding No. P1-0237). TT and MV would also like to acknowledge funding by the Slovenian Research Agency under grant number ARRS J7-2599. GJH was supported by the Austrian Science Fund (FWF) project number I 4978-B.

References

Amano, C., Zhao, Z., Sintes, E., Reinthaler, T., Stefanschitz, J., Kisadur, M., ... Herndl, G. J. (2022). Limited carbon cycling due to high-pressure effects on the deep-sea microbiome. *Nature Geoscience*, *15*, 1041-1047.

Bar-On, Y. M., Phillips, R., & Milo, R. (2018). The biomass distribution on earth. *Proceedings of the National Academy of Sciences*, *115*(25), 6506–6511.

Berelson, W. M. (2002). Particle settling rates increase with depth in the ocean.

Deep Sea Research Part II: Topical Studies in Oceanography, *49*(1-3), 237–251.

Billett, D., Bett, B., Jacobs, C., Rouse, I., & Wigham, B. (2006). Mass deposition of jellyfish in the deep arabian sea. *Limnology and Oceanography*, *51*(5), 2077–2083.

Boyd, P., & Trull, T. (2007). Understanding the export of biogenic particles in oceanic waters: Is there consensus? *Progress in Oceanography*, *72*(4), 276-312. Retrieved from `https://doi.org/10.1016/j.pocean.2006.10.007` doi: https://doi.org/10.1016/j.pocean.2006.10.007

Boyd, P. W., Claustre, H., Levy, M., Siegel, D. A., & Weber, T. (2019). Multi-faceted particle pumps drive carbon sequestration in the ocean. *Nature*, *568*(7752), 327-335. Retrieved from `https://doi.org/10.1038/s41586-019-1098-2` doi: https://doi.org/10.1038/s41586-019-1098-2

Briggs, N., Dall'Olmo, G., & Claustre, H. (2020). Major role of particle fragmentation in regulating biological sequestration of co¡sub¿2¡/sub¿ by the oceans. *Science*, *367*(6479), 791-793. doi: 10.1126/science.aay1790

Burd, A. B., Hansell, D. A., Steinberg, D. K., Anderson, T. R., Arístegui, J., Baltar, F., ... Tanaka, T. (2010). Assessing the apparent imbalance between geochemical and biochemical indicators of meso- and bathypelagic biological activity: What the @$#! is wrong with present calculations of carbon budgets? *Deep Sea Research Part II: Topical Studies in Oceanography*, *57*(16), 1557-1571. Retrieved from `https://doi.org/10.1016/j.dsr2.2010.02.022` (Ecological and Biogeochemical Interactions in the Dark Ocean) doi: https://doi.org/10.1016/j.dsr2.2010.02.022

Center, N. G. D. (2006). *2-minute Gridded Global Relief Data (ETOPO2) v2.* doi: 10.7289/V5J1012Q

Guidi, L., Legendre, L., Reygondeau, G., Uitz, J., Stemmann, L., & Henson, S. A. (2015). A new look at ocean carbon remineralization for estimating deep-water sequestration. *Global Biogeochemical Cycles*, *29*(7), 1044-1059. doi: https://doi.org/10.1002/2014GB005063

Henson, S. A., Sanders, R., & Madsen, E. (2012). Global patterns in efficiency of particulate organic carbon export and transfer to the deep ocean. *Global Biogeochemical Cycles*, *26*(1).

Herndl, G. J., & Reinthaler, T. (2013). Microbial control of the dark end of the biological pump. *Nature Geoscience*, *6*(9), 718-724. Retrieved from `https://doi.org/10.1038/ngeo1921` doi: https://doi.org/10.1038/ngeo1921

Hindmarsh, A. C. (1983). Odepack, a systematized collection of ode solvers. *IMACS Transactions on Scientific Computation*, *1*, 55-64.

Hoving, H.-J., Boetius, A., Dunlop, K., Greinert, J., Haeckel, M., Jones, D. O. B., ... Purser, A. (2023). Major fine-scale spatial heterogeneity in accumulation of gelatinous carbon fluxes on the deep seabed. *Frontiers in Marine Science*, *10*. doi: 10.3389/fmars.2023.1192242

Iversen, M. H. (2023). Carbon export in the ocean: A biologist's perspective. *Annual Review of Marine Science*, *15*(1), 357-381. doi: 10.1146/annurev-marine-032122-035153

Johnson, W. M., Longnecker, K., Kido Soule, M. C., Arnold, W. A., Bhatia, M. P., Hallam, S. J., ... Kujawinski, E. B. (2020). Metabolite composition of sinking particles differs from surface suspended particles across a latitudinal transect in the south atlantic. *Limnology and Oceanography*, *65*(1), 111-127. Retrieved from `https://doi.org/10.1002/lno.11255` doi: https://doi.org/10.1002/lno.11255

Lebrato, M., & Jones, D. (2009). Mass deposition event of pyrosoma atlanticum carcasses off ivory coast (west africa). *Limnology and Oceanography*, *54*(4), 1197–1209.

Lebrato, M., Molinero, J.-C., Cartes, J., Lloris, D., Mélin, F., & Beni-Casadella,

L. (2013). Sinking jelly-carbon unveils potential environmental variability along a continental margin. *PLoS ONE*, *8*(12), e82070. Retrieved from https://doi.org/10.1371/journal.pone.0082070 doi: https://doi.org/10.1371/journal.pone.0082070

Lebrato, M., Pahlow, M., Frost, J. R., Küter, M., de Jesus Mendes, P., Molinero, J.-C., & Oschlies, A. (2019). Sinking of gelatinous zooplankton biomass increases deep carbon transfer efficiency globally. *Global Biogeochemical Cycles*, *33*(12), 1764-1783. Retrieved from https://doi.org/10.1029/2019GB006265 doi: https://doi.org/10.1029/2019GB006265

Lebrato, M., Pitt, K. A., Sweetman, A. K., Jones, D. O., Cartes, J. E., Oschlies, A., ... others (2012). Jelly-falls historic and recent observations: a review to drive future research directions. *Hydrobiologia*, *690*, 227–245.

Lucas, C. H., Jones, D. O., Hollyhead, C. J., Condon, R. H., Duarte, C. M., Graham, W. M., ... Regetz, J. (2014). Gelatinous zooplankton biomass in the global oceans: geographic variation and environmental drivers. *Global Ecology and Biogeography*, *23*(7), 701–714.

Luo, J. Y., Condon, R. H., Stock, C. A., Duarte, C. M., Lucas, C. H., Pitt, K. A., & Cowen, R. K. (2020). Gelatinous zooplankton-mediated carbon flows in the global oceans: A data-driven modeling study. *Global Biogeochemical Cycles*, *34*(9), e2020GB006704. Retrieved from https://doi.org/10.1029/2020GB006704 doi: https://doi.org/10.1029/2020GB006704

Martin, J. H., Knauer, G. A., Karl, D. M., & Broenkow, W. W. (1987). Vertex: carbon cycling in the northeast pacific. *Deep Sea Research Part A. Oceanographic Research Papers*, *34*(2), 267-285. doi: https://doi.org/10.1016/0198-0149(87)90086-0

Middelburg, J. J. (2019). *Marine carbon biogeochemistry: a primer for earth system scientists*. Springer Nature.

Petzold, L. R. (1983). Automatic selection of methods for solving stiff and nonstiff systems of ordinary differential equations. *Siam Journal on Scientific and Statistical Computing*, *4*, 136-148.

Steinberg, D. K., & Landry, M. R. (2017). Zooplankton and the ocean carbon cycle. *Annual Review of Marine Science*, *9*(1), 413-444. Retrieved from 10.1146/annurev-marine-010814-015924 doi: 10.1146/annurev-marine-010814-015924

Tinta, T., Klun, K., & Herndl, G. J. (2021). The importance of jellyfish–microbe interactions for biogeochemical cycles in the ocean. *Limnology and Oceanography*, *66*(5), 2011-2032. Retrieved from https://doi.org/10.1002/lno.11741 doi: https://doi.org/10.1002/lno.11741

Turner, J. T. (2015). Zooplankton fecal pellets, marine snow, phytodetritus and the ocean's biological pump. *Progress in Oceanography*, *130*, 205-248. Retrieved from https://doi.org/10.1016/j.pocean.2014.08.005 doi: https://doi.org/10.1016/j.pocean.2014.08.005

Wright, R. M., Le Quéré, C., Buitenhuis, E., Pitois, S., & Gibbons, M. J. (2021). Role of jellyfish in the plankton ecosystem revealed using a global ocean biogeochemical model. *Biogeosciences*, *18*(4), 1291–1320.

Yang, P. J., Lemons, M., & Hu, D. L. (2018). Rowing jellyfish contract to maintain neutral buoyancy. *Theoretical and Applied Mechanics Letters*, *8*(3), 147-152. Retrieved from https://doi.org/10.1016/j.taml.2018.03.001 doi: https://doi.org/10.1016/j.taml.2018.03.001

Figure 1.

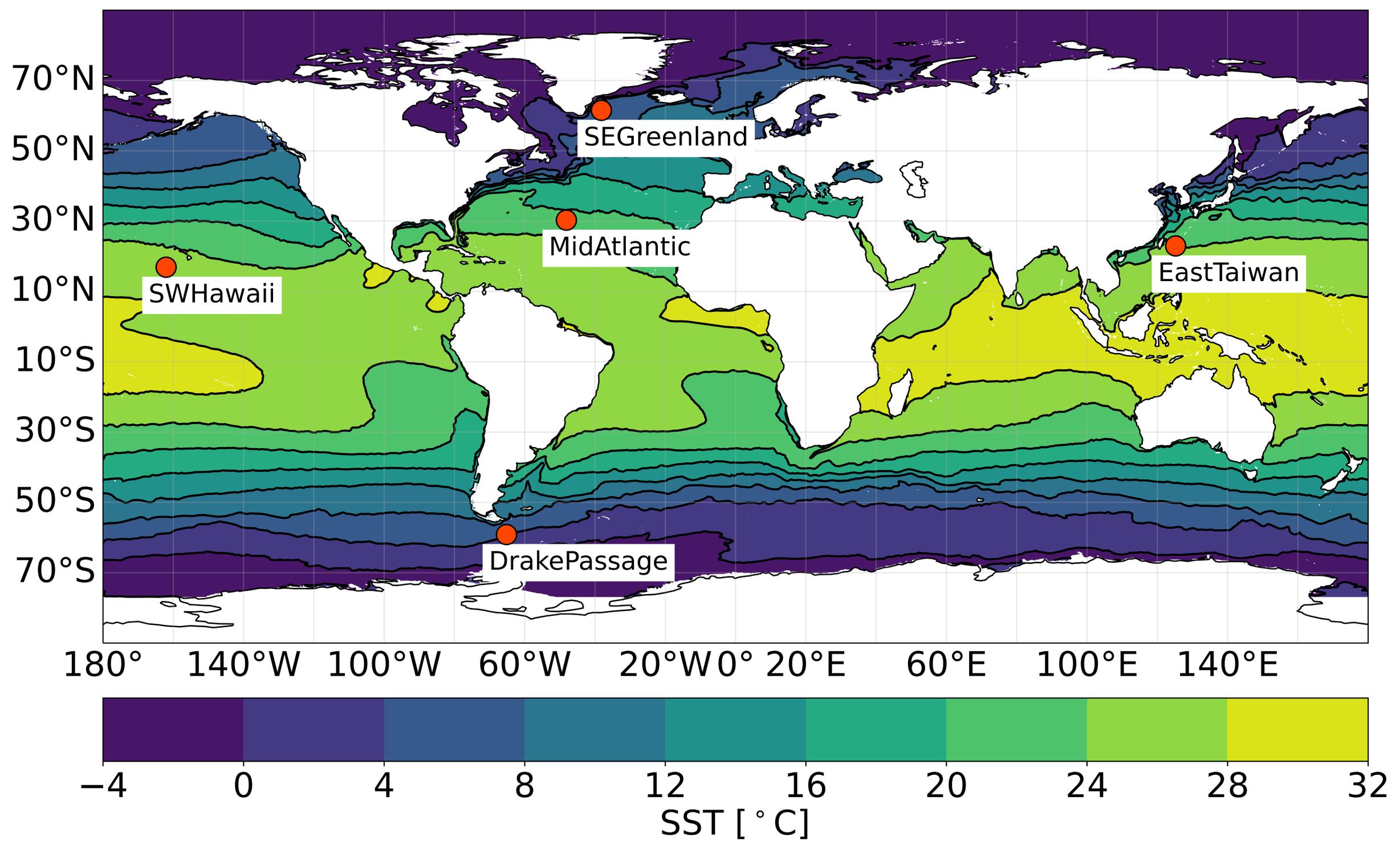
70°N
50°N
30°N
10°N
10°S
30°S
50°S
70°S
SEGreenland
MidAtlantic
SWHawaii
EastTaiwan
DrakePassage
180°
140°W
100°W
60°W
20°W
0°
20°E
60°E
100°E
140°E
−4
0
4
8
12
16
20
24
28
32
SST [° C]

Figure 2.

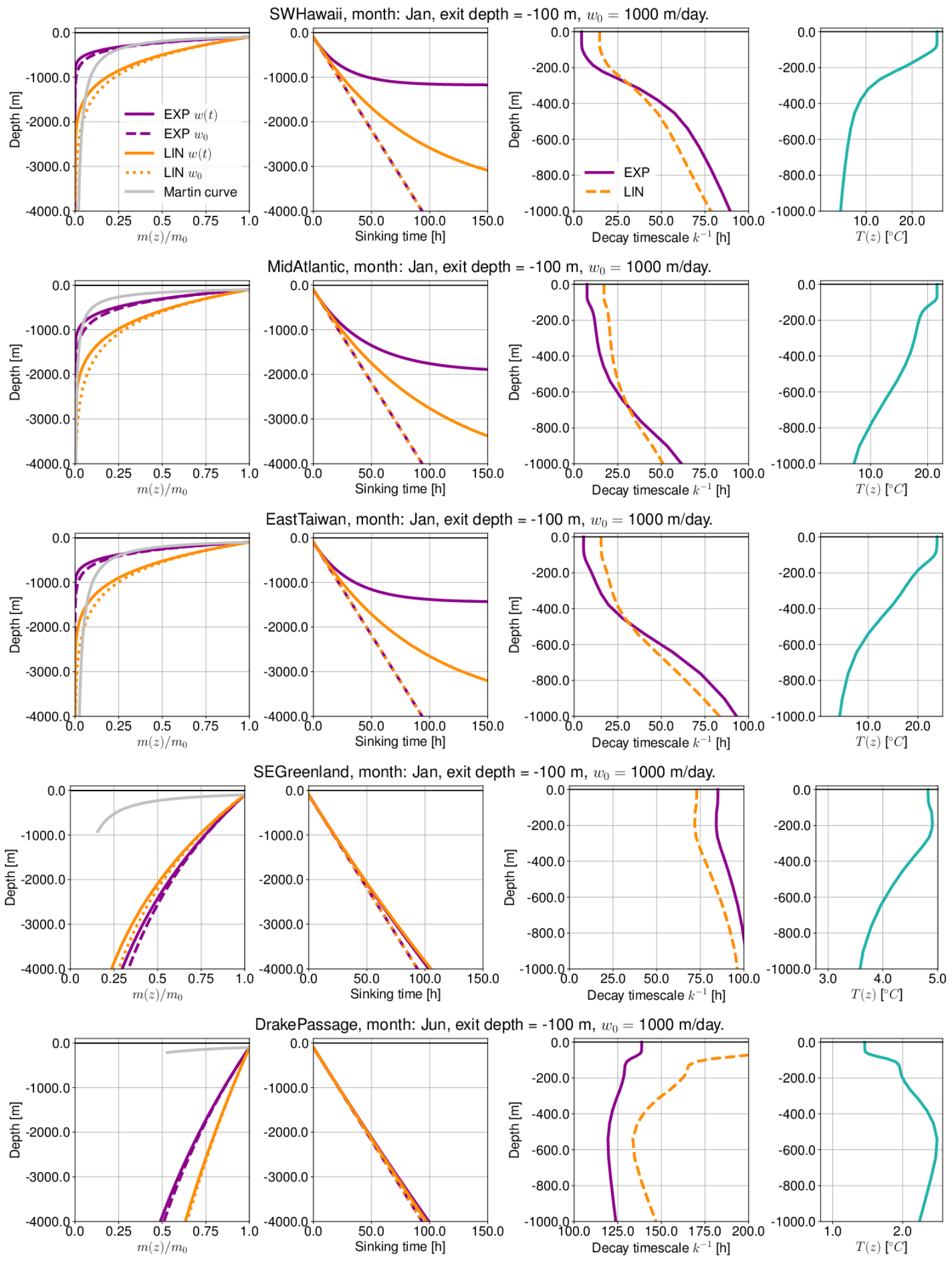
SWHawaii, month: Jan, exit depth = -100 m, w_0 = 1000 m/day.
MidAtlantic, month: Jan, exit depth = -100 m, w_0 = 1000 m/day.
EastTaiwan, month: Jan, exit depth = -100 m, w_0 = 1000 m/day.
SEGreenland, month: Jan, exit depth = -100 m, w_0 = 1000 m/day.
DrakePassage, month: Jun, exit depth = -100 m, w_0 = 1000 m/day.
Depth [m]
$m(z)/m_0$
EXP $w(t)$
EXP w_0
LIN $w(t)$
LIN w_0
Martin curve
Sinking time [h]
Decay timescale k^{-1} [h]
EXP
LIN
$T(z)$ [°C]

Figure 3.

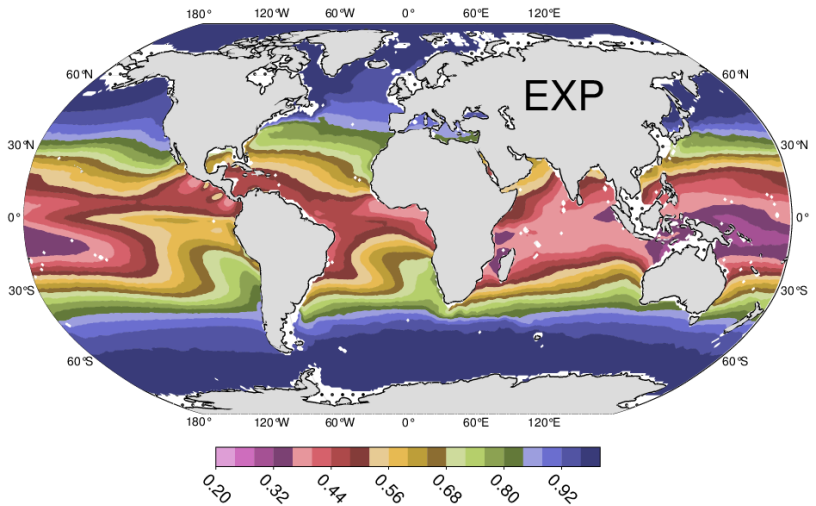

Fraction of mass m/m_0 at depth -200 m. Exit depth: 100 m. Month: Jan.

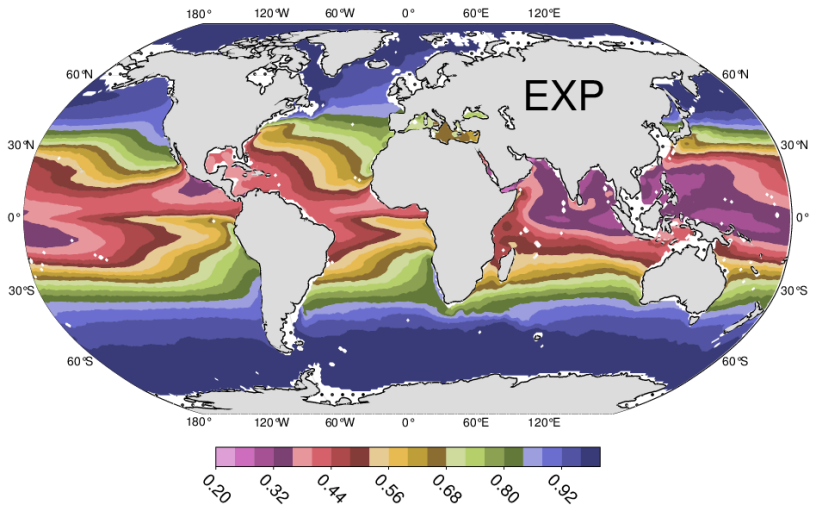

Fraction of mass m/m_0 at depth -200 m. Exit depth: 100 m. Month: Jun.

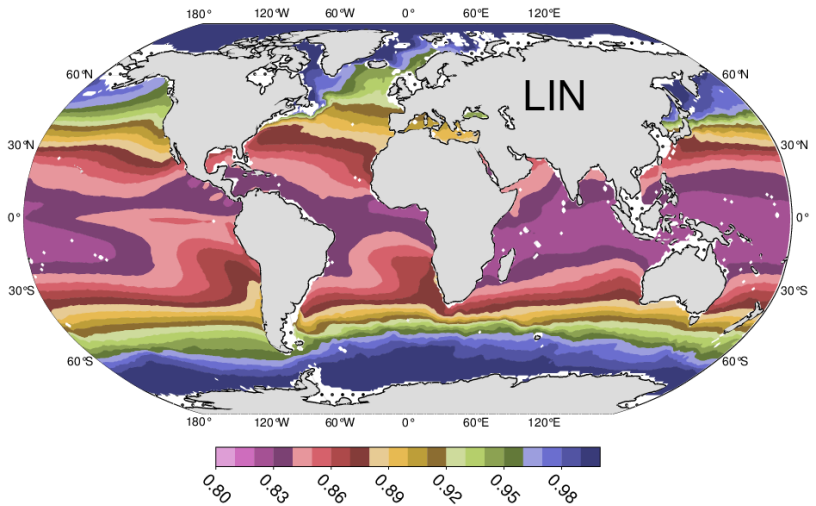

Fraction of mass m/m_0 at depth -200 m. Exit depth: 100 m. Month: Jan.

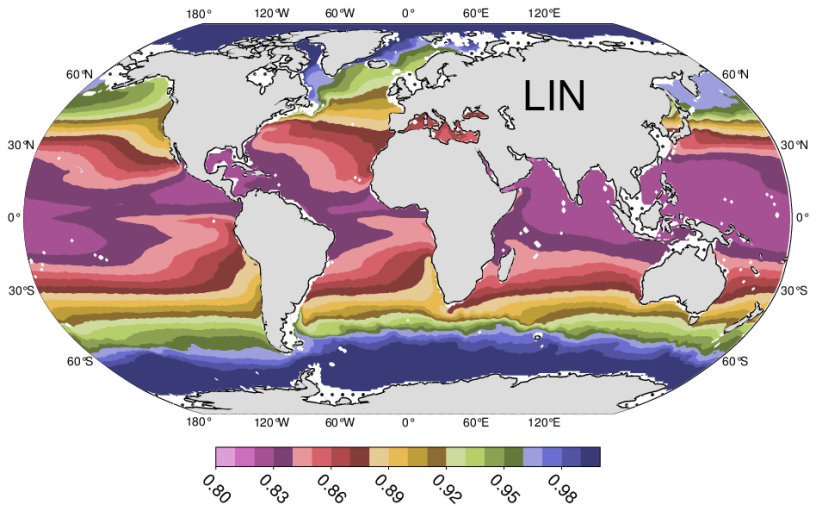

Fraction of mass m/m_0 at depth -200 m. Exit depth: 100 m. Month: Jun.

Figure 4.

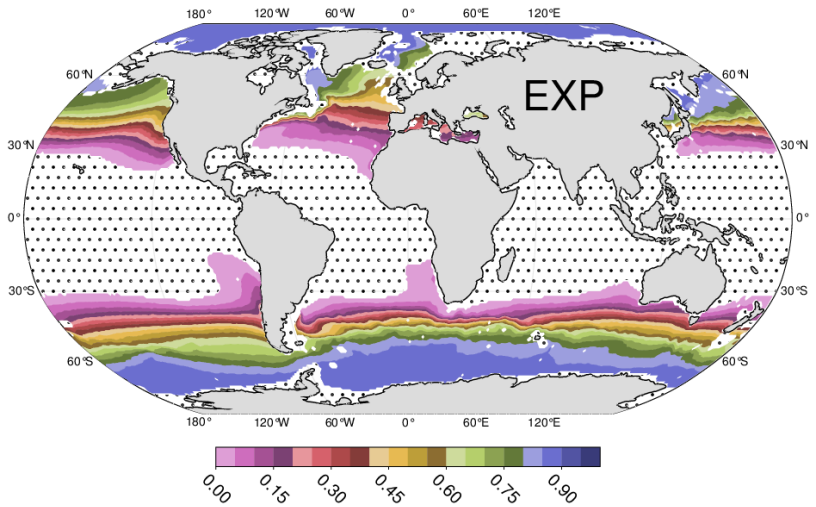

Fraction of mass m/m_0 at depth -1000 m. Exit depth: 100 m. Month: Jan.

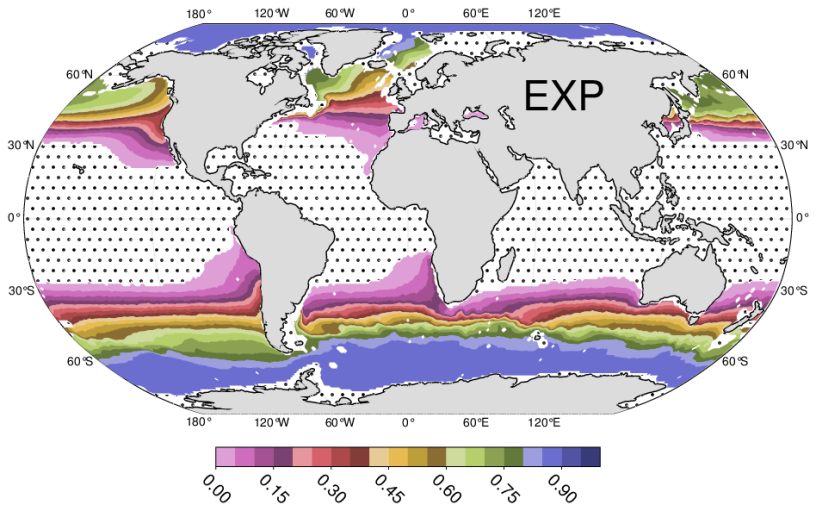

Fraction of mass m/m_0 at depth -1000 m. Exit depth: 100 m. Month: Jun.

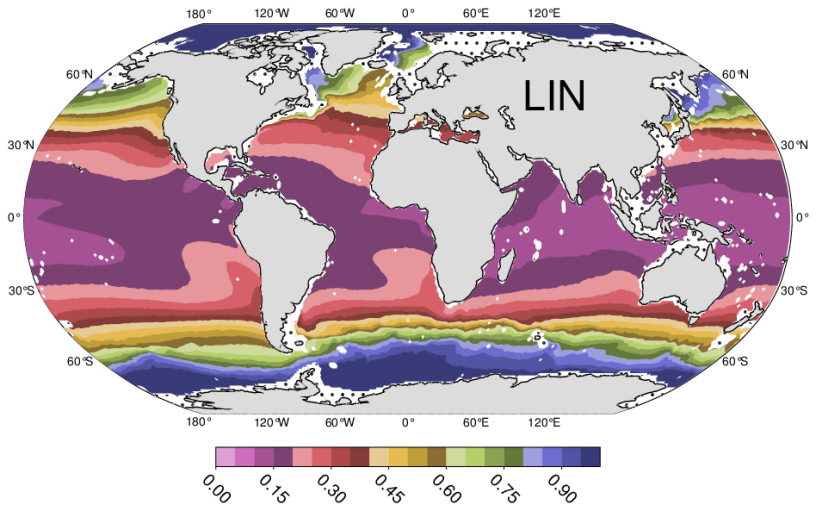

Fraction of mass m/m_0 at depth -1000 m. Exit depth: 100 m. Month: Jan.

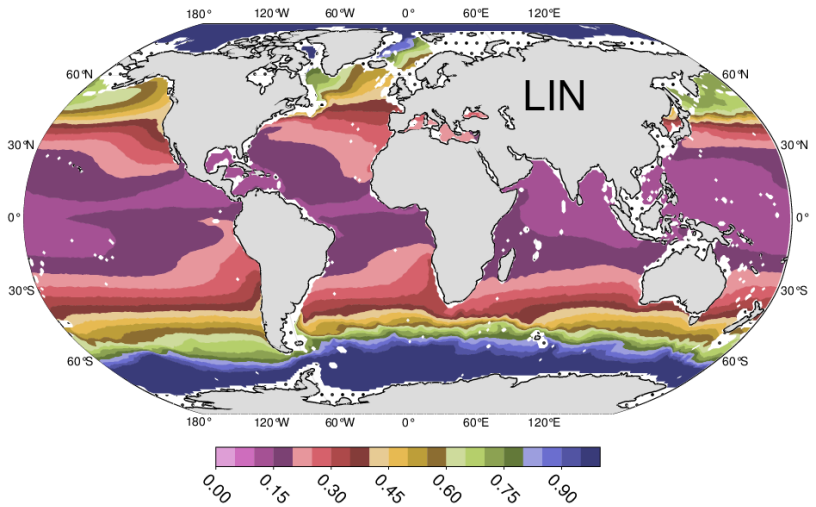

Fraction of mass m/m_0 at depth -1000 m. Exit depth: 100 m. Month: Jun.

Figure 5.

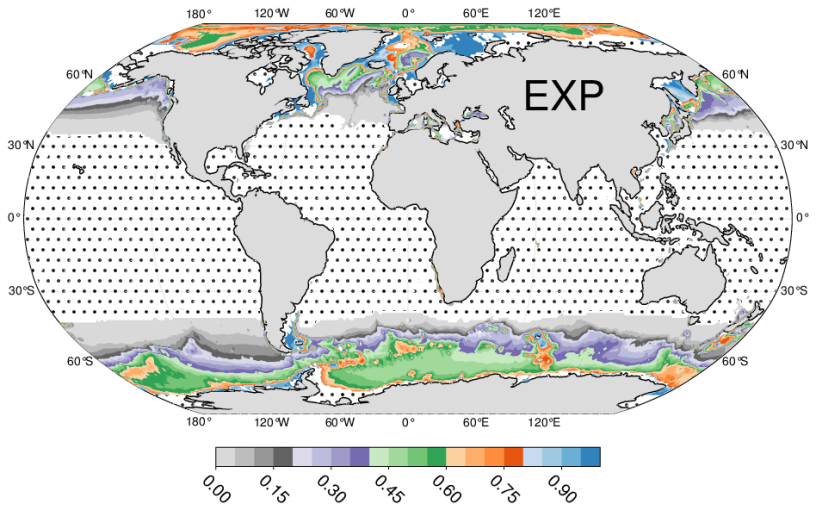

Mass fraction at ocean floor. Exit depth: 100 m. Month: Jan.

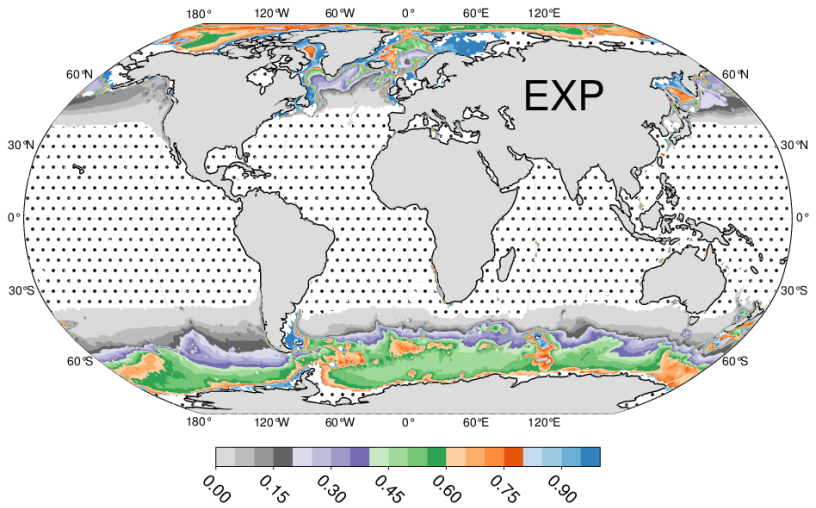

Mass fraction at ocean floor. Exit depth: 100 m. Month: Jun.

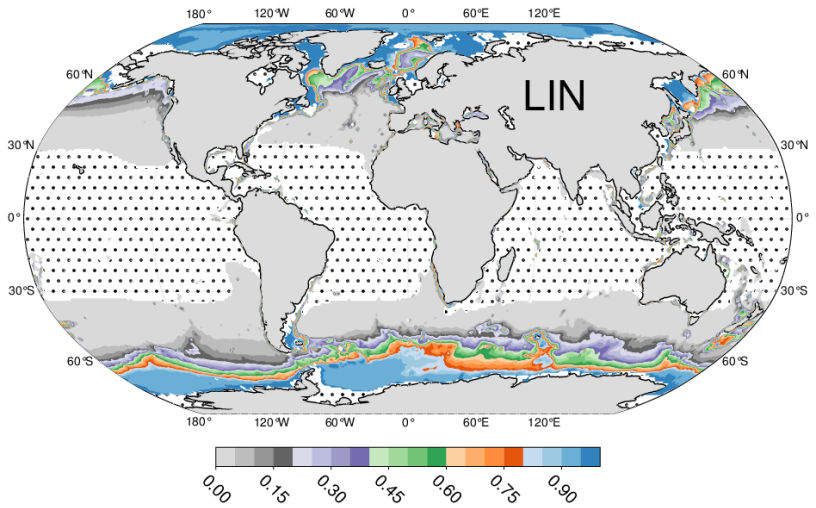

Mass fraction at ocean floor. Exit depth: 100 m. Month: Jan.

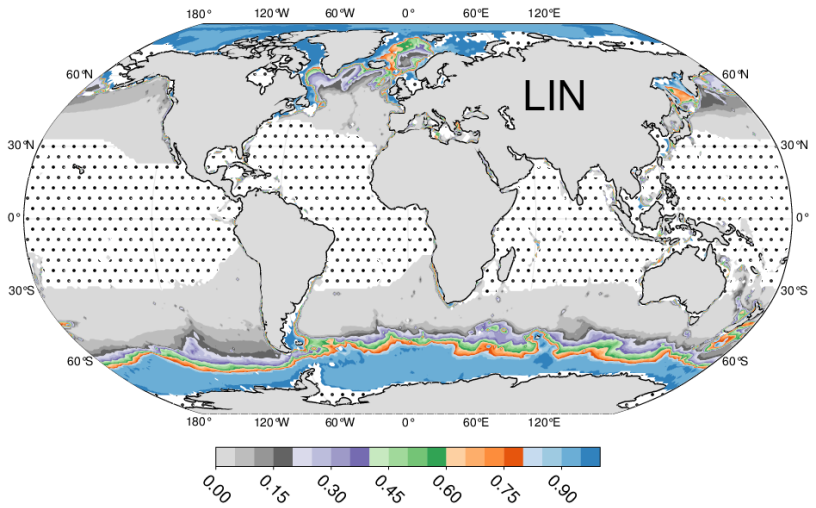

Mass fraction at ocean floor. Exit depth: 100 m. Month: Jun.

Figure 6.

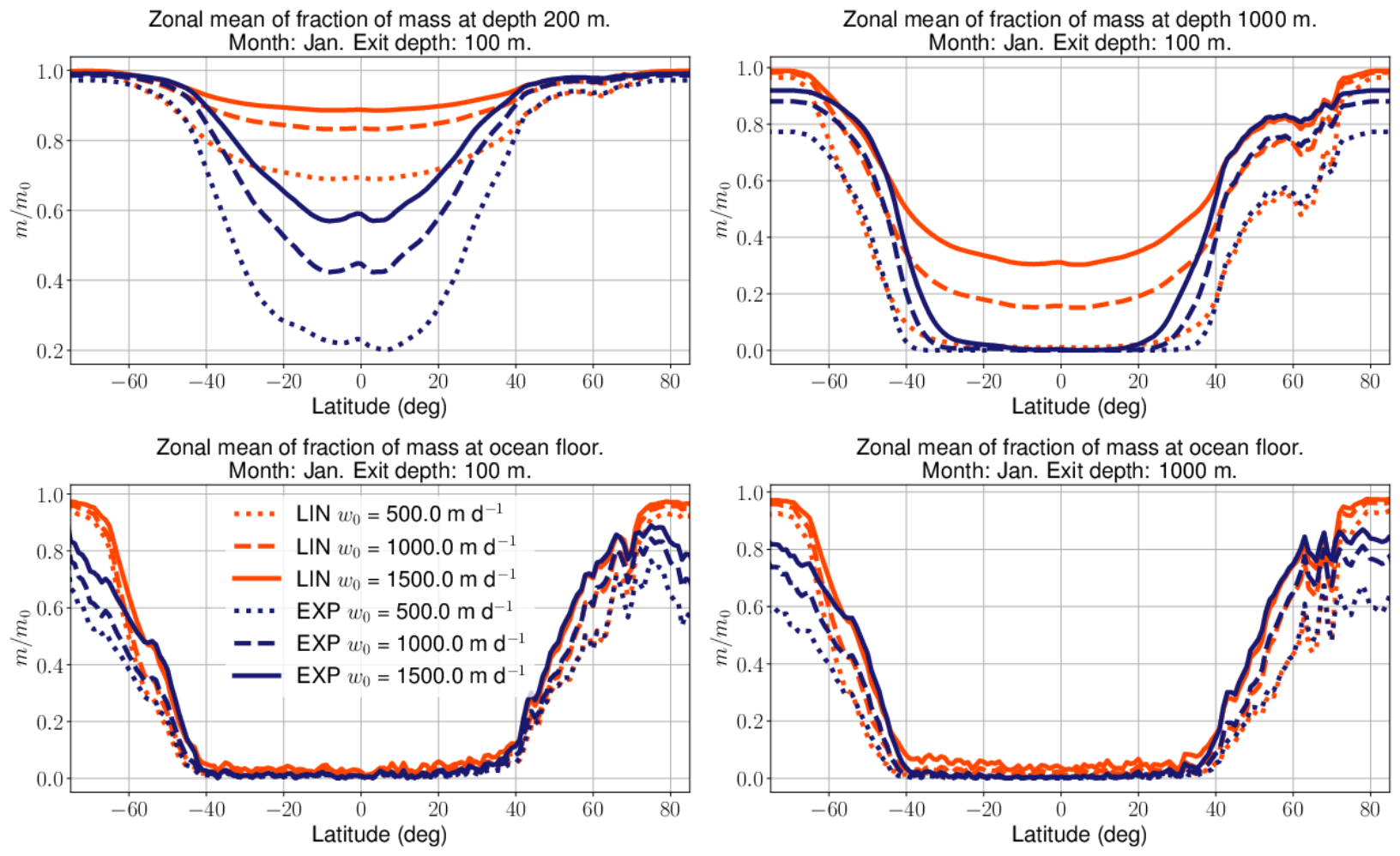
Zonal mean of fraction of mass at depth 200 m.
Month: Jan. Exit depth: 100 m.
Zonal mean of fraction of mass at depth 1000 m.
Month: Jan. Exit depth: 100 m.
Zonal mean of fraction of mass at ocean floor.
Month: Jan. Exit depth: 100 m.
Zonal mean of fraction of mass at ocean floor.
Month: Jan. Exit depth: 1000 m.
m/m_0
Latitude (deg)
LIN w_0 = 500.0 m d^{-1}
LIN w_0 = 1000.0 m d^{-1}
LIN w_0 = 1500.0 m d^{-1}
EXP w_0 = 500.0 m d^{-1}
EXP w_0 = 1000.0 m d^{-1}
EXP w_0 = 1500.0 m d^{-1}